THE JOURNAL OF PHYSICAL CHEMISTRY C

Article

pubs.acs.org/JPCC

Theoretic Insight into the Desulfurization Mechanism: Removal of H_2S by Ceria (110)

Senpeng Zhao,[†] Lixia Ling,[†] Baojun Wang,*[,‡,§] Riguang Zhang,[‡] Debao Li,[⊥] Qiang Wang,[⊥] and Jiancheng Wang[‡]

[†]Research Institute of Special Chemicals, Taiyuan University of Technology, Taiyuan 030024, Shanxi, People's Republic of China

[‡]Key Laboratory of Coal Science and Technology (Taiyuan University of Technology), Ministry of Education and Shanxi Province, Taiyuan 030024, Shanxi, People's Republic of China

[§]State Key Laboratory of Fine Chemicals, Dalian University of Technology, Dalian 116024, Liaoning, People's Republic of China

[⊥]State Key Laboratory of Coal Conversion, Institute of Coal Chemistry, Chinese Academy of Sciences, Taiyuan 030001, Shanxi, People's Republic of China

ABSTRACT: The periodic DFT+*U* calculation has been carried out to elucidate the desulfurization mechanism of H_2S with the ceria (110) surface. The calculations show that the H_2S molecule dissociatively adsorbs on the stoichiometric and reduced ceria (110) surfaces, respectively. The desulfurization process with the ceria (110) surface mainly contains two steps. First of all, H_2S interacts with the stoichiometric surface, and the SO_2-forming path is the most favorable reaction route based on the kinetics analysis. Meanwhile, surface O vacancies are created, and the reduced surface is formed. In this process, S in H_2S is transferred to another sulfur-containing compound, SO_2, which could not reduce the sulfur content in coal gas. Second, S in H_2S is captured by filling into the O vacancy and forming CeOS species on the reduced surface. Therefore, it can be inferred that the key to the desulfurization of H_2S in coal gas with ceria (110) is that more surface O vacancies are created.

1. INTRODUCTION

H_2S is the main sulfur compound in coal-derived gases, accounting for nearly 90%.[1] It is poisonous and corrosive and has negative effects on the industrial process, environment, and mankind's health.[2−7] Therefore, reducing the content of H_2S in gasified coal gas to the lowest possible concentration is indispensable before flowing to the downstream devices.

Ceria has been widely studied in environmental pollution control and catalysis; meanwhile, it has been investigated as a second-generation desulfurization sorbent to remove H_2S in coal-derived gas at high temperature.[8] Ceria desulfurizer has superior desulfurization performance, and the removal of H_2S to a lower level is achieved at high temperature.[8−12] Zeng et al.[8,9] discovered that the desulfurization capacity of the prereduced cerium oxides, CeO_n ($1.5 < n < 2$), is superior to the unreduced ceria, and the activity loss of the sorbent during 25 reduction−sulfurization−regeneration cycles is negligible. The desulfurization performance of ceria is closely correlated with its unique fluorite structure, and O vacancies can improve its desulfurization performance.[13] The interaction of H_2S with ceria was also studied by Mullins et al.[14] and Liu et al.,[15] and showed that different reaction products, S, H_2, H_2O, and SO_2, desorbed from ceria at different temperatures. Besides, the selectivity of sulfur and the stability of iron oxide catalyst were significantly improved by doping ceria, and a large amount of SO_2 was observed at the first stage with the 2Fe−2Ce catalyst in the absence of O_2.[16] SO_2 has a negative effect on the whole desulfurization process. However, to the best of our knowledge, the formation mechanism of SO_2 on the ceria surface is still unclear up to now.

The experimental information cannot completely and clearly elucidate the desulfurization mechanism. Lately, the density functional theory (DFT) method has already been extensively applied to provide insight into the reaction mechanism at a micromolecular level.[17−21] Chen et al.[17] studied the interaction mechanism between H_2S and the ceria (111) surface by using the DFT+*U* method and showed that the SO_2-forming pathway was the most favorable route based on the schematic potential energy profiles. In addition, the reduced ceria surface also plays a significant role in catalytic reactions. The dissociation of H_2S or H_2O in energetics was significantly affected by surface O vacancies on the ceria (111) surface,[22] and the interaction between water and ceria could be enhanced by surface O vacancies.[23−25] Meanwhile, our previous work demonstrated that the O-vacancy $Cu_2O(111)$ surface manifested stronger catalytic activity toward the dissociation of H_2S compared to the perfect and sulfur-containing surfaces.[21] The (110) surface of ceria is metastable among the low index surfaces, but it shows more catalytic activity and plays a more important role in catalytic oxidation reactions owing to its lowest O-vacancy

Received: November 11, 2014
Revised: March 18, 2015
Published: March 19, 2015

DOI: 10.1021/jp511289k
J. Phys. Chem. C 2015, 119, 7678−7688

formation energy.[26,27] It was found that ceria nanorods with (110) facets were more active than ordinary ceria nanoparticles with (111) facets in the CO−ceria interaction.[28,29] However, the interaction mechanisms between H_2S and the stoichiometric ceria (110) surface, as well as the reduced (110) surface, are still unclear. Therefore, a systemic study of the mechanism can provide helpful information for experimental studies focused on Ce-based catalyst designs.

The ceria (110) surface is the target of our current investigation in this work. The interaction mechanisms of H_2S with the stoichiometric and reduced ceria (110) surfaces are studied with the DFT+U calculation. Besides, we expect to elucidate three points in an atomistic level: (a) in terms of the stoichiometric and reduced ceria (110) surfaces, which one plays a more significant role in removing H_2S; (b) why the reduced ceria can improve the desulfurization performance; (c) the desulfurization mechanism of H_2S with the ceria (110) surface.

2. CALCULATION METHOD AND THE MODEL

2.1. Computation Method. Density functional theory (DFT) plane-wave calculations were performed using the Vienna ab initio simulation package (VASP)[30,31] with the projector-augmented wave (PAW)[32,33] method. The electron exchange and correlation were treated within the generalized gradient approximation (GGA), using the Perdew−Burke−Ernzerhof (PBE)[34] functional. A cutoff energy of 400 eV was used. The Brillouin zone integrations were performed using the Monkhorst−Pack grids[35] of 6 × 6 × 6 and 3 × 3 × 1 for the bulk and surface calculations, respectively. Geometry optimizations were considered converged when the forces on all free atoms were below 0.02 eV·Å^{-1}. Meanwhile, a Gaussian smearing parameter of SIGMA = 0.2 eV was used, and the spin polarization was performed in all calculations.

The DFT+U approach[36] was used in this work since the DFT method was unable to correctly describe the localization of the cerium 4f state.[27,37−39] A Hubbard parameter U value of 5.0 eV has been introduced to correct the strong on-site Coulomb interaction of Ce 4f electrons in previous works.[18,37,40−43] As such, we chose a value of U = 5.0 eV in this work. The optimized lattice parameter of the ceria bulk is 5.438 Å, which is in good agreement with the experimental value of 5.411 Å[44] and other calculated values.[18,26,45]

2.2. Surface Model. The slab model[46] was applied to investigate the interactions between the H_2S molecule and the stoichiometric and reduced ceria (110) surfaces. The stoichiometric ceria (110) surface was constructed with a supercell slab of 10.876 Å × 7.690 Å and five atomic layers, as shown in Figure 1. For the reduced ceria (110) surface, it was built by removing one O atom of the top layer from the stoichiometric surface. A vacuum thickness of 15 Å was employed to separate each slab from interactions. The bottom two layers for the five-layer slab were fixed at the optimized bulk position, and the remaining atoms were allowed to relax. The equilibrium geometries of the isolated S species and H atom were optimized in a cubic cell of 10 × 10 × 10 Å^3, and a larger cell of 15 × 15 × 15 Å^3 was used to optimize H_2O, SO_2, and H_2 molecules. The geometrical parameters of H_2S, H_2, H_2O, and SO_2 are listed in Table 1. It can be seen that the calculated results are well in line with the experimental data. Besides, Guo et al.[47] also used a cell of 10 × 10 × 10 Å^3 to optimize the isolated molecules in their calculations.

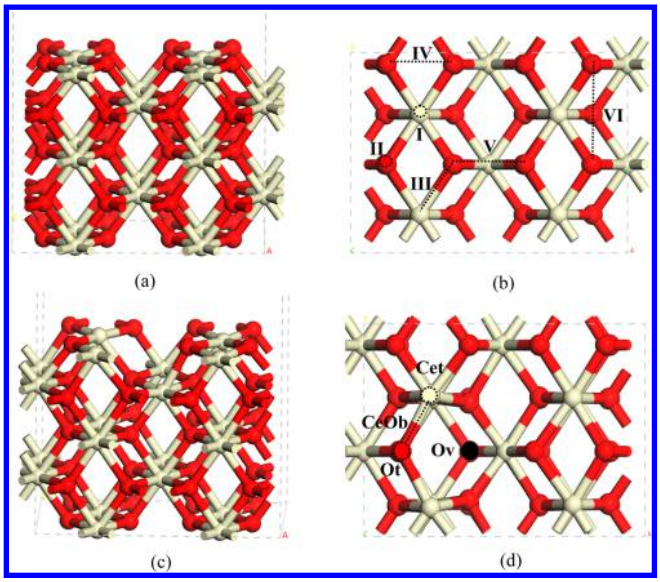

Figure 1. (a) Side and (b) top view of the stoichiometric ceria (110) surface. I, II, III, IV, V, and VI correspond to Ce-top, O-top, Ce−O bridge, O-st-O bridge, O-bg-O bridge, and O-lg-O bridge active sites, respectively. (c) Side and (d) top view of the reduced ceria (110) surface. Cet, Ot, CeOb, and Ov correspond to active sites for Ce-top, O-top, Ce−O, bridge and O-vacancy sites, respectively. Red and yellow spheres represent O and Ce atoms, respectively. Black ball stands for O vacancy site.

The adsorption energy is always recognized as a measurement of the intensity of the adsorbate−substrate interaction. The adsorption energy, E_{ads}, is defined as follows

$$E_{ads} = E_{ceria-adsorbate} - E_{ceria} - E_{adsorbate}$$

where $E_{ceria-adsorbate}$ is the total energy of the ceria (110) surface and adsorbate system in its equilibrium state; E_{ceria} is the energy of the ceria (110) surface; and $E_{adsorbate}$ is the energy of the isolated adsorbate. According to this definition, a more negative value reflects a stronger interaction between adsorbed species and the surface.

The formation energy of an O vacancy, E_v, is obtained by

$$E_v = E_{CeO_{2-x}} + \frac{1}{2}E_{O_2} - E_{CeO_2}$$

where $E_{CeO_{2-x}}$ is the total energy of the reduced ceria (110) surface. E_{CeO_2} is the total energy of the optimized stoichiometric ceria (110) surface, and E_{O_2} is the total energy for the ground state of an optimized O_2 molecule in the gas phase.

The climbing-image nudged elastic band (CI-NEB) method[48,49] was used to locate the transition states and map out the reaction pathways for H_2S dissociation and reaction on the ceria (110) surface. In the SO_2-forming path, the transition state was located by inserting four and eight images between the initial and the final states, respectively. Calculations showed that the difference of the energy barriers between these two methods was only 0.4 kJ·mol^{-1}, and the difference of the structure parameters was negligible. Therefore, four images could locate the transition state reliably. Besides, the method of inserting four images has been widely used to search the transition state in previous works.[18,50−53]

The rate constants k at different temperatures were estimated by using the harmonic transition state theory (TST)[54−56]

DOI: 10.1021/jp511289k
J. Phys. Chem. C 2015, 119, 7678−7688

Table 1. Calculated Geometrical Parameters of the Isolated Molecules Using the GGA-PBE+U Method

	H_2S		H_2		H_2O		SO_2	
	calcd	exptl[a]	calcd	exptl[a]	calcd	exptl[a]	calcd	exptl[a]
d^b (Å)	1.349	1.336	0.751	0.741	0.973	0.958	1.447	1.431
θ^c (deg)	91.63	92.12			104.45	104.51	119.21	119.33

[a]From ref 57. [b]The distances between atoms in S−H, H−H, H−O, and S−O bonds. [c]The bond angles of H−S−H, H−O−H, and O−S−O.

$$k = \frac{k_B T}{h}\frac{q_{TS}}{q_R}\exp\left(-\frac{E_a}{k_B T}\right)$$

where k_B is the Boltzmann constant; h is the Planck constant; T is the absolute temperature; E_a is the ZPVE-corrected activation energy; q_{TS} and q_R are the vibrational partition functions for the TS and reactant of every elementary step, respectively. For partition functions, q, the vibrational degrees of freedom are only considered in the surface reaction, and they are calculated in the harmonic model

$$q = \frac{1}{\prod_{i=1}^{\text{Vibrations}}\left[1 - \exp\left(-\frac{h\nu_i}{k_B T}\right)\right]}$$

where ν_i is the vibrational frequency.

3. RESULTS AND DISCUSSION

3.1. Assessment of the Surface Model. To confirm the sufficiency of the five-layer slab with the bottom two layers fixed (5−2−3 model), the larger models of seven atomic layers with the bottom two layers fixed (7−2−5 model) and four layers fixed (7−4−3 model) have also been built, and the adsorptions of H_2S, S, and H at the most stable adsorption sites on the seven-layer surface have been studied. The calculation shows that the differences of adsorption energies on these different surfaces are less than 1.0 kJ·mol^{-1}, as shown in Table 2. Therefore, the model of five atomic layers is sufficient to study the adsorption and reaction on the ceria (110) surface. In addition, Mei et al.[58] have also tested the influence of atomic layers with five, seven, and nine layers on the surface energies and found that the model with five atomic layers is sufficient to study the methanol decomposition process. The ceria (110) surface with five atomic layers has also been used to study SO_2 reduction, CO oxidation, CO_2 activation and dissociation on the surface and as a supporter.[18,59−62]

Table 2. Adsorption Energies (kJ·mol^{-1}) of H_2S, S, and H on the Different Models

	5−2−3 model	7−2−5 model	7−4−3 model
	E_{ads}	E_{ads}	E_{ads}
H_2S	−107.8	−107.3	−107.1
S	−299.3	−298.6	−298.7
H	−364.2	−363.5	−363.7

As for the reduced ceria (110) surface, the formation energy of an O vacancy on the top layer is 191.6 kJ·mol^{-1}, which is similar to the calculated values reported before[26,27,63,64] and is lower than that of other metal oxides surfaces.[65,66] Meanwhile, the structure with an O vacancy on the second layer was also built. However, the O vacancy formation energy is 268.3 kJ·mol^{-1}, which is higher than that on the top layer. It indicates that the formation of an O vacancy on the second layer is more difficult. Therefore, only the vacancy located on the top layer is considered in this study. Besides, the oxygen vacancy on the top layer has been widely investigated in the reported works,[42,64,67] while the study of that on the second layer is quite few.

3.2. Adsorptions of H_2S, SH, S, and H on the Stoichiometric Ceria (110) Surface. Six different active sites of the stoichiometric ceria (110) surface were taken into consideration, namely, "Ce-top", "O-top", "Ce−O bridge", "O-st-O bridge", "O-bg-O bridge" and "O-lg-O bridge", as illustrated in Figure 1b. The adsorptions of H_2S, SH, S, and H species at the above six sites were investigated with the DFT +U method.

3.2.1. H_2S Adsorption. In the case of H_2S adsorption on the stoichiometric ceria (110) surface, we investigate four adsorption modes by different orientations, H-down, 2H-down, S-down, and SH-down modes, meaning that one H atom, two H atoms, one S atom, or a SH group of H_2S molecules interact with different surface sites directly. There are three types of adsorption manners based on the optimized configurations: molecular adsorption, partially dissociative adsorption (dissociation into SH and H), and completely dissociative adsorption (dissociation into S and 2H), as depicted in Figure 2. Calculated adsorption energies suggest that H_2S mainly exists on the surface in the partially dissociative adsorption mode by one dissociated H atom adsorbing at the surface O and SH binding to the nearby surface Ce. As shown in configuration H_2S(a), one dissociated H atom of H_2S is bound to the surface O, and the forming H−O and the breaking S−H bond lengths are 0.986 and 3.355 Å, respectively. SH absorbs at the surface Ce with the S−Ce bond of 2.782 Å, and the S−H bond is slightly elongated to 1.351 Å compared to that of the free H_2S molecule (1.349 Å). The adsorption energy of this structure is −107.8 kJ·mol^{-1}. What's more, a hydrogen bond formed between O−H and the neighboring surface O makes the structure more stable. The dissociative adsorption mode is similar to the adsorption of H_2S on the ZnO($10\bar{1}0$) surface[19] but is different from that on the CeO_2(111),[17] Cu_2O(111),[21] and α-Fe_2O_3(0001)[20] surfaces with molecular adsorption. Besides, Mullins et al.[68] also discovered that H_2O dissociatedly adsorbed on the oxidized CeO_2(100) and (111) surfaces experimentally.

What is surprising is that the completely dissociative adsorption is also discovered with H_2S dissociation into S and two H atoms, when H_2S interacts with the O-st-O bridge and O-lg-O bridge sites with the 2H-down mode, as the structures of H_2S(b) and H_2S(c) in Figure 2. However, the adsorption energies of H_2S(b) and H_2S(c) (−38.8 and −59.4 kJ·mol^{-1}, respectively) are lower compared to that of the partially dissociative adsorption. It implies that the completely dissociative mode may be an important intermediate during the desulfurization of H_2S. As for H_2S(d), the molecular adsorption is that the H_2S molecule absorbs at the upside of the surface Ce and is nearly parallel to the surface. The distance of the S−Ce bond is 3.244 Å, and the S−H bond lengths are 1.354 and

DOI: 10.1021/jp511289k
J. Phys. Chem. C 2015, 119, 7678−7688

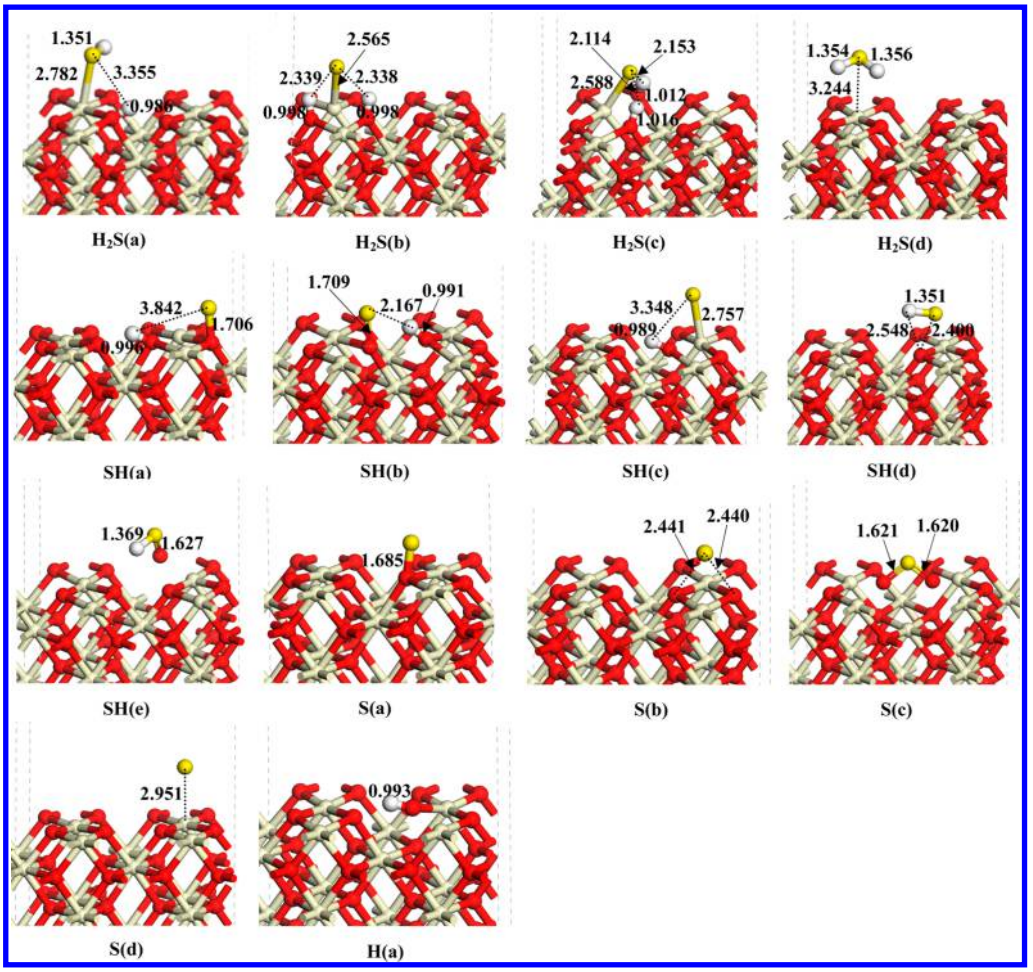

Figure 2. Geometric structures of H_2S, SH, S, and H adsorption on the stoichiometric ceria (110) surface optimized by using the DFT+*U* method.

1.356 Å, respectively. The adsorption energy is −27.5 kJ·mol^{-1}, belonging to the weak physical adsorption.

3.2.2. SH Adsorption. The interactions of SH with different sites of the stoichiometric ceria (110) surface are also examined in a similar manner to that of H_2S, and the optimized geometries and the corresponding adsorption energies are displayed in Figure 2 and Table 3, respectively. It can be observed that there are two adsorption forms: molecular adsorption and dissociative adsorption. The most stable configuration is SH(a) with an adsorption energy of −262.5 kJ·mol^{-1}, where the breaking S−H bond is stretched to 3.842 Å and the separated S and H atoms bind to two neighboring O atoms of the O-st-O bridge site, respectively. The forming S−O and H−O bond lengths are 1.706 and 0.996 Å, respectively. As for SH(b), the dissociated S and H bind to O atoms of the O-bg-O bridge site with an adsorption energy of −257.2 kJ·mol^{-1}, respectively. There is a little gap of 5.3 kJ·mol^{-1} between SH(a) and SH(b), indicating these two configurations can both stably exist. In SH(c), the dissociated S and H atoms are bound to the surface Ce and O, respectively. The breaking S−H bond is elongated to 3.348 Å, and the adsorption energy is −131.3 kJ·mol^{-1}, suggesting that the adsorption of the S atom at the surface Ce is not stable, and it may transfer to the surface O to form a more stable structure.

Table 3. Adsorption Energies (kJ·mol^{-1}) of H_2S, SH, S, and H on the Stoichiometric Ceria (110) Surface

	E_{ads}		E_{ads}		E_{ads}
H_2S(a)	−107.8	SH(a)	−262.5	S(a)	−299.3
H_2S(b)	−38.8	SH(b)	−257.2	S(b)	−134.4
H_2S(c)	−59.4	SH(c)	−131.3	S(c)	−392.4
H_2S(d)	−27.5	SH(d)	−102.7	S(d)	−72.6
		SH(e)	−187.2	H(a)	−364.2

The molecular adsorption structure is SH(d) with an adsorption energy of −102.7 kJ·mol^{-1}. SH adsorbs at the upside of the surface O and is nearly parallel to the surface, and the S−H bond is 1.351 Å. Somewhat unexpectedly, one O atom is dragged out of the surface by SH, forming O−SH species, when the S atom of SH interacts with the surface O, as shown in SH(e). This may be caused by the high activity of the surface O and the strong interaction force between S and O atoms.

3.2.3. Atomic S and H Adsorption. In the case of atomic S, the S atom is initially placed at the Ce−O or O-lg-O bridge site, and it diffuses to the surface O after optimization. S binds to the surface O with an adsorption energy of −299.3 kJ·mol^{-1}, and the bond length of S−O is 1.685 Å, as S(a) depicted in Figure 2. This structure is different from the structures of atomic S absorbing on other metal oxide surfaces, on which the metal[20,21] or metal−O bridge[17,19] sites are the most stable absorption sites for the S atom. In the configurations of S(b) and S(d), atomic S adsorbs at the O-st-O bridge and Ce-top sites with the adsorption energies of −134.4 and −72.6 kJ·mol^{-1}, respectively. Nevertheless, when the S atom is located at

DOI: 10.1021/jp511289k
J. Phys. Chem. C 2015, 119, 7678−7688

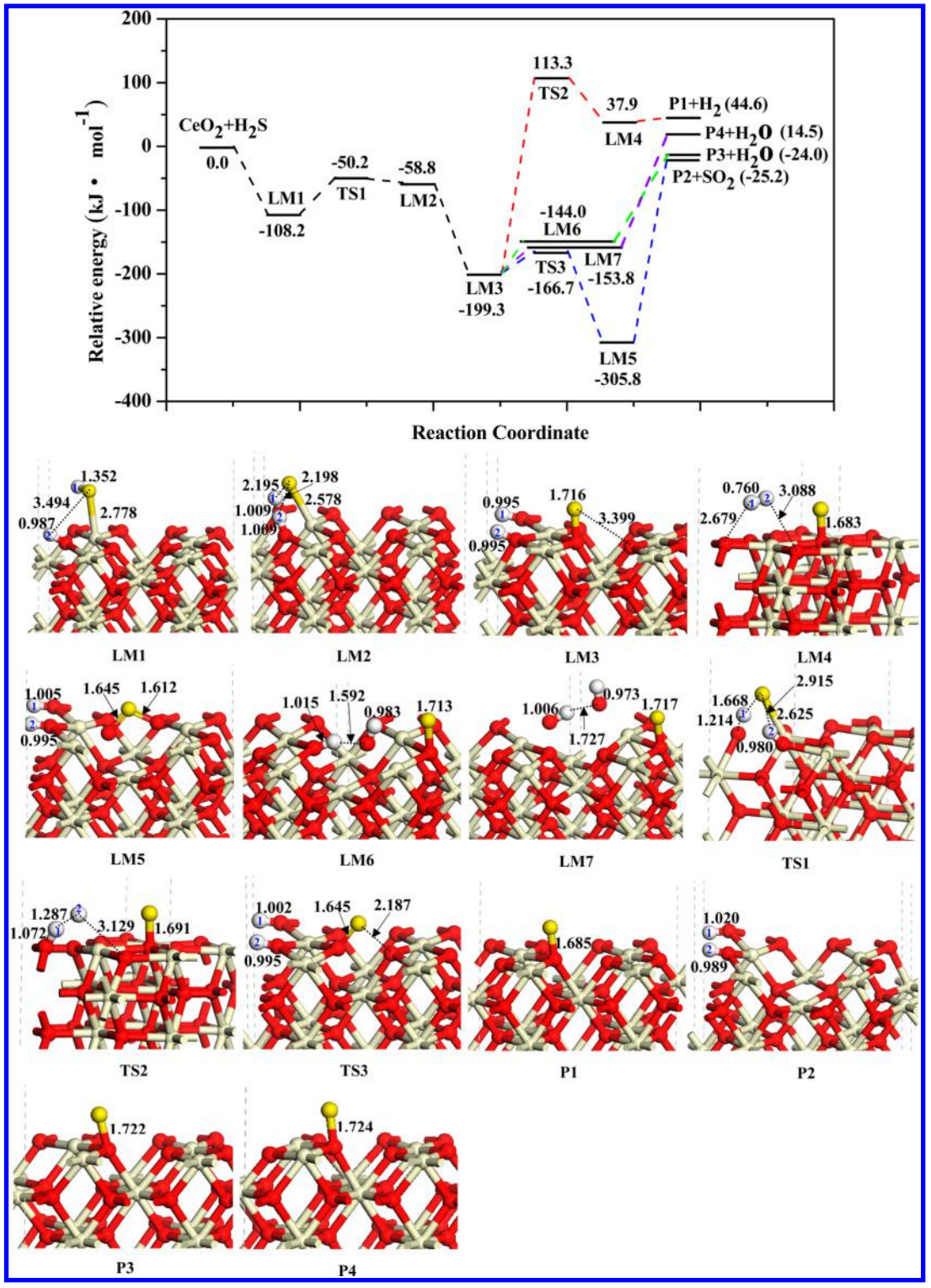

Figure 3. Schematic potential energy profiles and the structures of intermediates, transition states, and products for the interaction between H_2S and the stoichiometric ceria (110) surface.

the O-bg-O bridge site, it interacts with two neighboring O atoms and pulls them out of the surface, producing SO_2 species, showing that the surface O atom is quite active. We suppose that the stably adsorbed S atom in structure S(a) may easily shift to the O-bg-O bridge site to form SO_2 species, which may be an important reaction product for H_2S interaction with the stoichiometric ceria (110) surface. As for atomic H, H prefers to adsorb at the surface O by forming surface hydroxyl, which is similar to H adsorbing on other metal oxides,[17,19−21] as H(a) shows in Figure 2. The adsorption energy of this structure is −364.2 kJ·mol^{-1}, and the O−H bond length is 0.993 Å.

3.3. Reaction Mechanism between H_2S and the Stoichiometric Ceria (110) Surface. With respect to the reaction mechanism of H_2S with the stoichiometric ceria (110) surface, a detailed investigation has been conducted, and four steps are mainly considered: (a) the dissociation of H_2S on the

DOI: 10.1021/jp511289k
J. Phys. Chem. C 2015, 119, 7678−7688

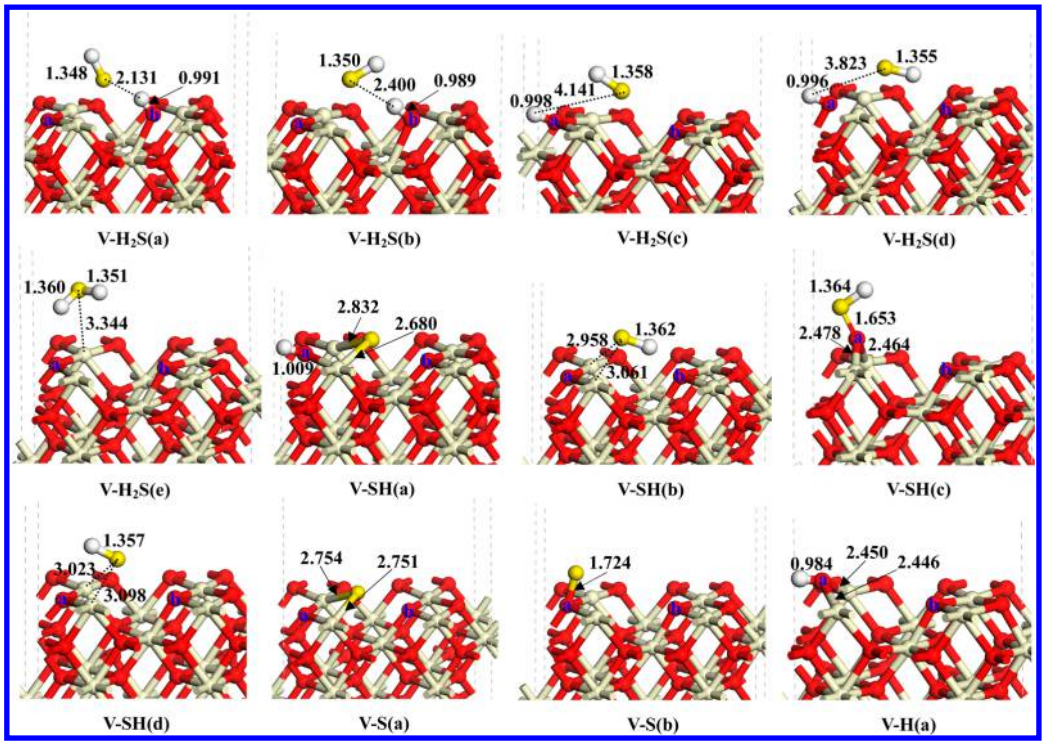

Figure 4. Geometric structures of H_2S, SH, S, and H adsorption on the reduced ceria (110) surface optimized by the DFT+*U* method.

surface; (b) the interaction of two dissociated H atoms to form a H_2 molecule; (c) the formation of H_2O by two dissociated H atoms interacting with one surface O; (d) the release of SO_2 by S of H_2S capturing two surface O atoms.

The result presented above shows that the partially dissociative adsorption of H_2S predominantly occurs on the stoichiometric ceria (110) surface. The first dehydrogenation process ($H_2S \rightarrow SH + H$) can spontaneously take place without additional energy under the catalysis of ceria, and an important intermediate LM1 is formed with an exothermicity of 108.2 kJ·mol^{-1}. The schematic potential energy profiles for the interaction based on the CI-NEB calculations are displayed in Figure 3. Meanwhile, the optimized geometries of the intermediates (LM), transition states (TS), and products (P) are also illustrated. Besides, two H atoms of H_2S are labeled as H1 and H2 to more clearly characterize the whole reaction process.

Starting from LM1, the second dehydrogenation step takes place ($SH1 \rightarrow S + H1$), by overcoming a reaction energy barrier of 58.0 kJ·mol^{-1} at TS1, producing LM2 with an endothermicity of 49.4 kJ·mol^{-1}. The bond length of S−H1 elongates from 1.352 Å in LM1 via 1.668 Å in TS1 to 2.195 Å in LM2, while the distance of S−Ce is shortened from 2.778 Å in LM1 via 2.625 in TS1 to 2.578 Å in LM2. The O−H1 bond length in TS1 is 1.214 Å. The S atom prefers to interact with the surface O on the basis of the aforementioned discussion, so the formation of a stable S−O bond is investigated by the S atom in LM2 transferring to the neighboring O atom, and the S−O bond (1.716 Å) in LM3 is elongated compared to that of one single S atom adsorbing on the surface (1.685 Å). However, there is no transition state discovered from LM2 to LM3, indicating that the transformation can occur spontaneously with a high exothermicity of 140.5 kJ·mol^{-1}.

The H_2S molecule can easily dissociate into S and two H atoms based on the above discussion, and S and H atoms are inclined to bind to the surface O atoms. Nevertheless, the reaction products, H_2, H_2O and SO_2, have been observed during the interaction between H_2S and ceria in experiments.[14,15] Koyuncu et al.[16] also detected the SO_2 product on the Ce−Fe mixed oxide catalyst. In addition, Chen et al.[17] have studied three reaction channels for H_2S interaction with the stoichiometric ceria (111) surface, producing H_2, H_2O, and SO_2. Therefore, the formation processes of H_2, H_2O, and SO_2 on the stoichiometric ceria (110) surface are also studied in this work to clearly describe the interaction mechanisms. As show in Figure 3, the LM3 intermediate can undergo a H_2-forming process giving LM4 via TS2 with a high reaction barrier of 312.6 kJ·mol^{-1}, indicating that the H−O bond is fairly stable and the formation of H_2 is quite difficult. The distances of H1−O and H2−O in TS2 are elongated to 1.072 and 3.129 Å, respectively. The bond length of H1−H2 in LM4 is 0.760 Å, which is slightly longer than that of the free H_2 molecule (0.751 Å, see Table 1). Then the weakly bound H_2 can desorb barrierlessly to produce H_2 and P1. The whole pathway is endothermic by 44.6 kJ·mol^{-1}. Meanwhile, the formation of H_2O has been studied, and the O-vacancy surface is formed followed by the release of H_2O. The adsorption of H_2O on the defected surface is investigated first. However, the H_2O molecule is inclined to dissociatively adsorb on the defected surface by one H atom of the H_2O molecule migrating to the neighboring surface O and forming two surface OH groups, as LM6 and LM7 shown in Figure 3. It suggests that the formation of H_2O is impossible on the stoichiometric ceria (110) surface, and the dissociated H atoms mainly exist in the form of surface hydroxy groups. To more clearly describe the existential state of H_2O on the stoichiometric ceria (110) surface, the dissociative adsorption structures of LM6 and LM7 are listed on the potential energy profiles in Figure 3. Meanwhile, the O-vacancy surfaces with S adsorption are also displayed, as shown in P3 and P4. It implies that when the H_2O

DOI: 10.1021/jp511289k
J. Phys. Chem. C 2015, 119, 7678−7688

Table 4. Adsorption Energies (kJ·mol^{-1}) of H_2S, SH, S, and H on the Reduced Ceria (110) Surface

	E_{ads}		E_{ads}		E_{ads}
V−H_2S(a)	−155.3	V−SH(a)	−266.1	V−S(a)	−317.4
V−H_2S(b)	−159.3	V−SH(b)	−266.9	V−S(b)	−315.7
V−H_2S(c)	−178.0	V−SH(c)	−172.4	V−H(a)	−357.8
V−H_2S(d)	−185.5	V−SH(d)	−256.9		
V−H_2S(e)	−22.3				

molecule adsorbs on the O-vacancy surfaces with S, two OH groups are investigated instead of the H_2O molecule. However, the formation of the H_2O molecule can be obtained on the ZnO($10\bar{1}0$) and α-Fe_2O_3(0001) surfaces in our pervious calculations.[19,20] The calculated energy barriers for the formation of H_2 and H_2O on the ZnO($10\bar{1}0$) surface are 199.5 and 97.6 kJ·mol^{-1} from the same intermediate, respectively, while those on the α-Fe_2O_3(0001) surface are 145.4 and 142.8 kJ·mol^{-1}, respectively. As for the formation of SO_2, a low reaction barrier of 32.6 kJ·mol^{-1} is needed to overcome at TS3, generating LM5, and this step is exothermic by 106.5 kJ·mol^{-1} in excess of the reaction barrier. This implies that SO_2 is formed easily. The bond lengths of S−O in LM5 are 1.645 and 1.612 Å, respectively, which are longer than that of the free SO_2 molecule (1.447 Å). Then the formed SO_2 molecule desorbs from the surface, producing SO_2 and P2. The overall reaction energy for the formation of SO_2 and P2 is exothermic by 25.2 kJ·mol^{-1}.

On the basis of the above molecular level calculation, it demonstrates that the SO_2-forming process is the most probable reaction route for the interaction between H_2S and the stoichiometric ceria (110) surface in kinetics, due to the high active surface O of ceria. This is similar to that on the stoichiometric ceria (111) surface by the DFT+U method.[17] The formation of SO_2 results in the loss of two O atoms on the surface, forming a defected surface. Surface defects may play an important role in various catalytic reactions, and the O-vacancy ceria can significantly promote the interaction of H_2O with ceria.[22−25] In addition, the S atom of H_2S is transferred to SO_2, which could not reduce the sulfur content in coal gas. Therefore, the role of O vacancy in the desulfurization needs to be studied and analyzed in the following.

3.4. Adsorption of H_2S, SH, S, and H on the Reduced Ceria (110) Surface. According to the above study, we can see that the O vacancy can be easily formed on the ceria (110) surface. Here, we use the in-plane-vacancy surface to study the adsorption and dissociation of H_2S on the defected surface. As illustrated in Figure 1(d), four adsorption sites are taken into consideration, including Ce-top, O-top, Ce−O bridge, and O-vacancy sites, since the remainder of the surface is structurally identical to the stoichiometric ceria (110) surface. All of the optimized structures are shown in Figure 4, while Table 4 displays the adsorption energies of H_2S, SH, S, and H on the reduced ceria (110) surface.

3.4.1. H_2S Adsorption. The adsorptions of H_2S at different sites of the reduced ceria (110) surface have been investigated. It indicates that H_2S prefers to bind to the surface in a dissociative adsorption mode, which is comparable to the adsorptions of H_2S on the O-deficient ZnO($10\bar{1}0$)[69] and O-vacancy Cu_2O(111)[21] surfaces. The dissociated H atom is bound to two surface O atoms around the O-vacancy site, namely, O_a and O_b, while S−H adsorbs at the O-vacancy site in different orientations, as shown in Figure 4. It can be observed that more H_2S molecules dissociated leading to the formation of −OH and −SH with 20% of Ce^{4+} reduced to Ce^{3+} on the ceria (111) surface,[14] and H_2O dissociatively adsorbed on the reduced ceria (100) and (111) surfaces in experiment.[68] The adsorption energies of V−H_2S(a), V−H_2S(b), V−H_2S(c), and V−H_2S(d) are −155.3, −159.3, −178.0, and −185.5 kJ·mol^{-1}, respectively, which are much higher than that on the stoichiometric surface, suggesting that the O-vacancy surface is conducive to the adsorption of the H_2S molecule. Besides, the structure of H adsorbing at O_a is more stable than that at O_b. The most stable configuration is V−H_2S(d), in which the distance between the dissociated H and S atoms is 3.823 Å, and the second is V−H_2S(c). As for V−H_2S(e), the H_2S molecule binds to the surface Ce atom with a lower adsorption energy of −22.3 kJ·mol^{-1}, belonging to the weak physical adsorption. The S−H bonds are elongated to 1.351 and 1.360 Å, respectively, compared to that of the free H_2S molecule in the gas phase.

3.4.2. SH Adsorption. In the same manner, the interactions of SH with different sites of the reduced ceria (110) surface are also examined. The optimized geometries and calculated adsorption energies are shown in Figure 4 and Table 4, respectively. As for V−SH(a), we can see that SH is dissociatively adsorbed on the surface with a high adsorption energy of −266.1 kJ·mol^{-1}. The H atom is bound to the surface O, while the S atom migrates to the O vacancy site and the sulfide surface is formed. In V−SH(b) and V−SH(d), the SH molecule adsorbs at the O-vacancy site by the H atom toward O_b and O_a with the adsorption energies of −266.9 and −256.9 kJ·mol^{-1}, respectively. The bond lengths of S−H are 1.362 and 1.357 Å, respectively. In the configuration V−SH(c), SH is bound to O_a with the S−O_a bond of 1.653 Å. The surface is distorted, and O_a transfers to the middle of two Ce atoms. However, the adsorption energy of V−SH(c) is only −172.4 kJ·mol^{-1}, indicating that V−SH(c) is less stable compared to the above three geometries. Therefore, the most stable adsorption structure is V−SH(b), and the second is V-SH(a); however, there is only a slight difference of 0.8 kJ·mol^{-1} between them.

3.4.3. Atomic S and H Adsorption. The S atom is initially placed at the Ce-top and Ce−O bridge sites, and it diffuses to the O-vacancy site after optimization, as V−S(a) seen in Figure 4. The S atom fills into the O vacancy to form the sulfide structure with the Ce−S bond lengths of 2.754 and 2.751 Å, respectively. The adsorption energy is −317.4 kJ·mol^{-1}. In V−S(b), the S atom stably binds to the surface O_a with the S−O_a bond length of 1.724 Å. The adsorption energy is −315.7 kJ·mol^{-1}, which is slightly higher compared to that of V−S(a). With respect to H adsorption, the most stable structure is V−H(a), where the H atom adsorbs at O_a with an adsorption energy of −357.8 kJ·mol^{-1}. The surface is distorted, and the O_a atom moves up from the surface. Hence, the most stable adsorption site of atomic S on the reduced ceria (110) surface is the O-vacancy site, while that of the H atom is the surface O.

3.5. Reaction Mechanism between H_2S and the Reduced Ceria (110) Surface. Similar to the stoichiometric ceria (110) surface, the reaction mechanism of H_2S with the

DOI: 10.1021/jp511289k
J. Phys. Chem. C 2015, 119, 7678−7688

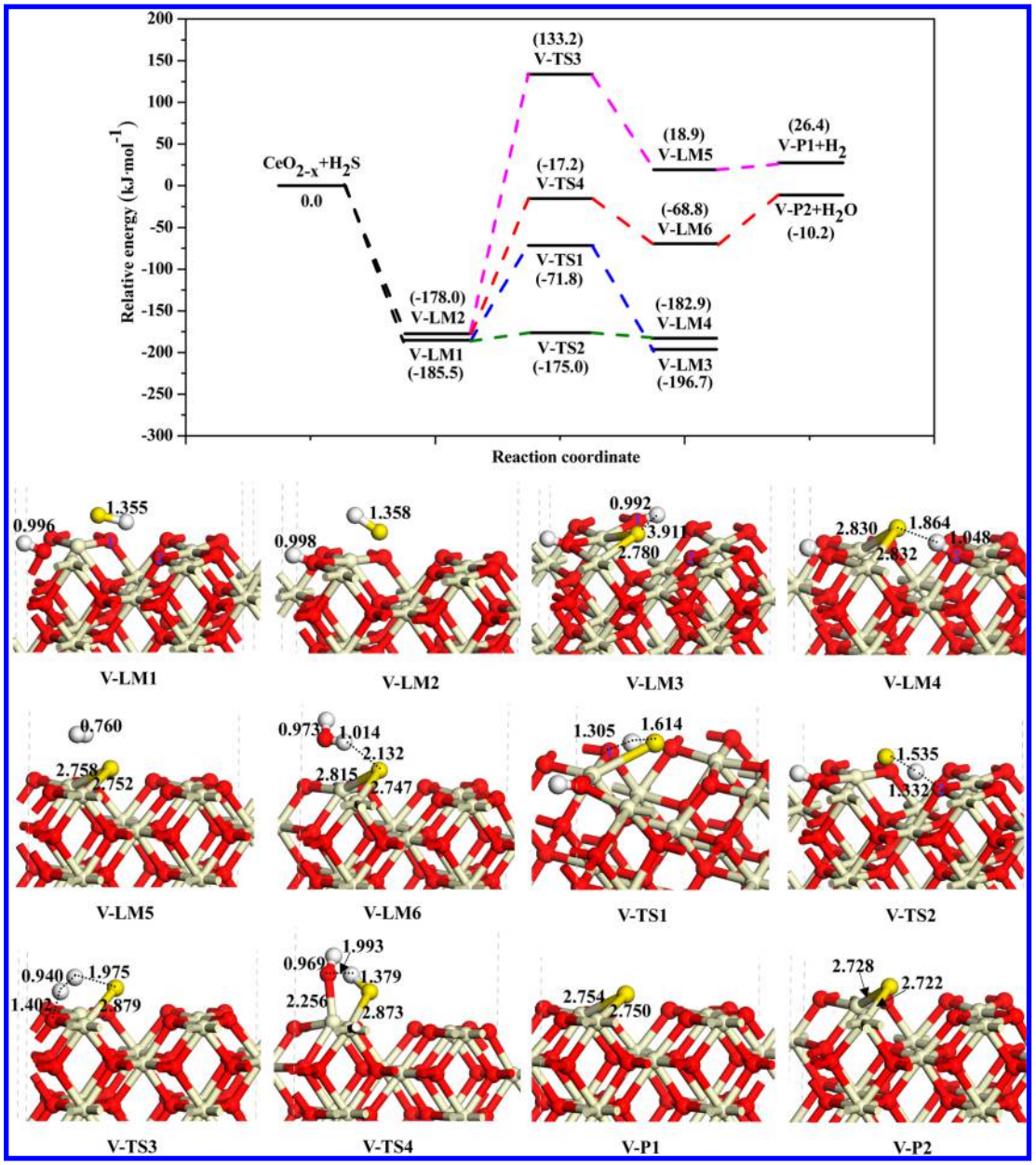

Figure 5. Schematic potential energy profiles and the structures of intermediates, transition states, and products for the interaction between H_2S and the reduced ceria (110) surface.

reduced ceria (110) surface has been systematically discussed in this work. As discussed above, the H_2S molecule can spontaneously dissociate into SH and H on the reduced surface during the first dehydrogenation process ($H_2S \rightarrow SH + H$). We choose the stable adsorption structures of V−H_2S(d) and V−H_2S(c) in energetics as the initial states V-LM1 and V-LM2 to study the whole processes, respectively. The schematic potential energy profiles for the processes based on the CI-NEB calculations are displayed in Figure 5.

As for the second dehydrogenation step ($SH \rightarrow S + H$), we choose V-LM1 as an initial state and consider two dehydrogenation paths because the dissociated H atom may shift to the far surface O_1 producing V-LM3 or transfer to the nearest surface O_2 forming V-LM4, as shown in Figure 5. From V-LM1 to V-LM3, a transition state V-TS1 is searched with a reaction energy barrier of 113.7 kJ·mol^{-1}, which is higher than that on the perfect surface. The S−H bond in V-TS1 is elongated by 0.259 Å compared to that in V-LM1 (1.355 Å), whereas the O_1−H bond is shortened to 1.305 Å at V-TS1. The breaking S−H and the forming O−H bond in V-LM3 are 3.911 and 0.992 Å, respectively. The other path is that the H atom of SH migrates to the nearest surface O_2 site by overcoming an energy barrier of 10.5 kJ·mol^{-1} in V-TS2, forming V-LM4. This energy barrier is even lower compared to the first path and that on the perfect surface. The S−H and O_2−H bond lengths in V-TS2 are 1.535 and 1.332 Å, respectively. These two reaction paths are exothermic by 196.7 and 182.9 kJ·mol^{-1}, respectively. Meanwhile, both of the dissociated S atoms of SH fill into the O-vacancy sites, leading to the formation of CeOS species on the surface. Besides, the H atom in SH prefers to migrate to the nearest surface O_2 site with a quite lower energy barrier.

In addition, atomic S prefers to adsorb at the O-vacancy site, and producing three surface O vacancies will make the surface quite unstable during the SO_2-forming process on the reduced

DOI: 10.1021/jp511289k
J. Phys. Chem. C 2015, 119, 7678−7688

Table 5. Rate Constants for the Main Reaction Steps of Different Products at Different Temperatures on the Stoichiometric and Reduced Ceria (110) Surfaces

		rate constant ln k (s^{-1})				
main reaction step	E_a [a]	300 K	600 K	900 K	1200 K	1500 K
LM1 → LM2	59.7	3.23	15.08	19.17	21.31	22.66
LM3 → LM4	270.5	−79.45	−24.30	−5.62	3.89	9.68
LM3 → LM5	30.4	18.04	24.97	27.44	28.76	29.61
V-LM2 → V-LM5	283.2	−83.11	−25.57	−6.16	3.68	9.66
V-LM2 → V-LM6	149.6	−26.96	4.56	15.33	20.81	24.16

[a]ZPVE corrected activation energy in kJ·mol^{-1}.

surface. Therefore, the SO_2-forming process is not considered in this work. However, with respect to H atoms of H_2S, the formation mechanisms of H_2 and H_2O on the reduced ceria (110) surface have been discussed by using V-LM2 as the initial state, and the correspondingly schematic potential energy profiles and structures are demonstrated in Figure 5. The V-LM2 intermediate can undergo a H_2-formation process by H of SH interacting with the surface H atom, producing V-LM5. However, a fairly high energy barrier of 311.2 kJ·mol^{-1} is required to be overcome in V-TS3, which is similar to that on the stoichiometric ceria (110) surface. The bond lengths of O−H, S−H, and H−H in V-TS3 are 1.402, 1.975, and 0.940 Å, respectively. The bond length of H_2 in V-LM5 is 0.760 Å, which is slightly longer than that of the free H_2 molecule. Finally, the H_2 molecule desorbs from the surface, producing V−P1, and the surface is sulfurized by forming CeOS species. The H_2-forming pathway is endothermic by 26.4 kJ·mol^{-1}. Besides, the H atom of SH can react with the surface hydroxyl to produce H_2O by overcoming an energy barrier of 160.8 kJ·mol^{-1} in V-TS4. The bond lengths of O−H and S−H in the configuration V-TS4 are 1.993 and 1.379 Å, respectively. Finally, the H_2O molecule desorbs from V-LM6, forming V−P2, while the S atom fills into the O vacancy and bonds to the surface Ce atoms with the Ce−S bond lengths of 2.728 and 2.722 Å, giving rise to the formation of the sulfide surface. The overall H_2O-formation process is exothermic by 10.2 kJ·mol^{-1}.

We can clearly draw a conclusion that S atoms fill into the O-vacancy sites, and the surface sulfide products, CeOS species, are produced on the reduced ceria (110) surface, regardless of whether the dehydrogenation processes or the H_2-forming and the H_2O-forming processes take place. The formation of the sulfide surface is conducive to remove H_2S molecules in coal gas, and it can account for why the reduced ceria can improve the desulfurization efficiency in experiments.[8,13]

3.6. Kinetic Analysis for the Desulfurization Processes on the Ceria (110) Surface. The rate constants ln k for the main reaction steps of different products on the stoichiometric and reduced ceria (110) surfaces at five different temperatures (300, 600, 900, 1200, and 1500K) are shown in Table 5. It can be concluded that the rate constant for the formation of SO_2 from LM3 to LM5 on the stoichiometric surface is larger than that for the dissociation of SH (LM1 → LM2). It implies that the dissociation of SH into S and H atoms is the rate-determining step. The rate constant for the formation of H_2 (LM3 → LM4) is rather smaller compared to that of SO_2. On the reduced surface, the rate constant for the formation of H_2O (V-LM2 → V-LM6) is rather larger than that of H_2 (V-LM2 → V-LM5), suggesting that the formation of H_2 is quite difficult. Therefore, SO_2 and H_2O are the main reaction products for the interaction of H_2S with the stoichiometric and reduced ceria (110) surfaces, respectively. H_2 may be produced at quite high temperatures on both surfaces. The rate constants ln k for the main reaction steps also increase with the temperature increasing. Liu et al.[15] studied the adsorption and reaction of H_2S on ceria and found that SO_2 desorbed between 473 and 673 K, while the sulfate was formed by SO_2 reacting with lattice oxygen at above 673 K. Mullins et al.[14] also discovered that H_2O was produced near 580 K with 20% of Ce^{4+} reduced to Ce^{3+}, while the formation of H_2O was suppressed and H_2 desorbed with 70% of Ce^{4+} reduced.

3.7. Difference between Ceria and Other Desulfurizers. On the basis of the above discussion, we suppose that the desulfurization process with the ceria (110) surface mainly contains two steps. First, the H_2S molecule interacts with the stoichiometric surface and converts to SO_2 species. Meanwhile, surface O vacancies are created, and the reduced surface is formed due to the high active surface O of ceria. Furthermore, the S in H_2S is captured by filling into the O vacancy and forming CeOS species on the reduced surface to achieve the goal of removing H_2S. This is markedly different from other desulfurizers. Previous DFT calculations showed that atomic S of H_2S mainly adsorbed on the perfect α-$Fe_2O_3(0001)$,[20] $ZnO(10\bar{1}0)$,[19] and $Cu_2O(111)$[21] surfaces by forming S-metal species, suggesting that these perfect surfaces can remove H_2S directly. Therefore, it can be inferred that ceria being prereduced under the reducing atmosphere to create more surface O vacancies is key to the desulfurization of H_2S in coal gas.

4. CONCLUSION

The periodic DFT+U calculation has been carried out to elucidate the desulfurization mechanism of H_2S with the ceria (110) surface. The adsorptions of H_2S, SH, atomic S, and H on the stoichiometric and reduced ceria (110) surfaces have been systematically investigated. The results show that H_2S is dissociatively adsorbed on both surfaces. The S atom is preferentially adsorbed at the O-bg-O site forming SO_2 species and at the O-vacancy site, respectively. Atomic H is inclined to bond to the surface O to form hydroxyl species.

On the stoichiometric surface, the surface adsorbates (S and H atoms) can further release H_2 or react with the surface O to form SO_2. On the basis of our calculations, H adsorbates prefer to exist in the form of surface hydroxyl, and the SO_2-forming process is the most favorable reaction route in kinetics. However, the surface sulfide products, CeOS species, are produced by S atom filling into the O vacancy on the reduced surface, regardless of whether the dehydrogenation processes or the H_2-forming and the H_2O-forming processes take place. It is beneficial to remove H_2S gas and is well in line with the experiment.

DOI: 10.1021/jp511289k
J. Phys. Chem. C 2015, 119, 7678−7688

Being different from other absorbents, we speculate that the desulfurization process with ceria (110) mainly contains two steps. First, the H_2S molecule reacts with the stoichiometric surface and converts to SO_2 species. Meanwhile, surface O vacancies are created, and the reduced surface is produced. Furthermore, the S atom of H_2S is captured by S filling into the O vacancy and forming CeOS species on the reduced surface. This two-step mechanism can account for why reduced ceria can improve the desulfurization efficiency in experiment. Therefore, it can be inferred that the key to the desulfurization of H_2S in coal gas with ceria (110) is that more surface O vacancies are created.

AUTHOR INFORMATION

Corresponding Author

*Tel.: +86 351 6018239. Fax: +86 351 6041237. E-mail address: wangbaojun@tyut.edu.cn.

Notes

The authors declare no competing financial interest.

ACKNOWLEDGMENTS

We thankfully acknowledge financial support from the National Natural Science Foundation of China (Grant Nos. 21276171, 21276003), the National Younger Natural Science Foundation of China (Grant No. 21103120), China Postdoctoral Science Foundation (Grant No. 2012M520608), and the State Key Laboratory of Fine Chemicals (KF1205).

REFERENCES

(1) Xie, W.; Chang, L. P.; Yu, J. L.; Xie, K. C. Research Progress of the Removal of H_2S from Coal Gas by Dry Method. *J. Chem. Ind. Eng.* **2006**, *57*, 2012−2020.

(2) Rodriguez, J. A.; Hrbek, J. Interaction of Sulfur with Well-Defined Metal and Oxide Surfaces: Unraveling the Mysteries behind Catalyst Poisoning and Desulfurization. *Acc. Chem. Res.* **1999**, *32*, 719−728.

(3) Bain, R. L.; Dayton, D. C.; Carpenter, D. L.; Czernik, S. R.; Feik, C. J.; French, R. J.; Magrini−Bair, K. A.; Phillips, S. D. Evaluation of Catalyst Deactivation during Catalytic Steam Reforming of Biomass-Derived Syngas. *Ind. Eng. Chem. Res.* **2005**, *44*, 7945−7956.

(4) Sato, K.; Shinoda, T.; Fujimoto, K. New Nickel-Based Catalyst for Tar Reforming with Superior Resistance to Coking and Sulfur Poisoning in Biomass Gasification Processes. *J. Chem. Eng. Jpn.* **2007**, *40*, 860−868.

(5) Cheah, S.; Carpenter, D. L.; Magrini-Bair, K. A. Review of Mid- to High-Temperature Sulfur Sorbents for Desulfurzation of Biomass- and Coal-Derived Syngas. *Energy Fuel.* **2009**, *23*, 5291−5307.

(6) Yang, G. D.; Wu, L. Y.; Jiang, B.; Yang, W.; Qi, J. S.; Cao, K.; Meng, Q. H.; Mustafa, A. K.; Mu, W. T.; Zhang, S. M.; et al. H_2S as a Physiologic Vasorelaxant: Hypertension in Mice with Deletion of Cystathionine γ-Lyase. *Science* **2008**, *322*, 587−590.

(7) Johansen, D.; Ytrehus, K.; Baxter, G. F. Exogenous Hydrogen Sulfide (H_2S) Protects against Regional Myocardial Ischemia-Reperfusion Injury. *Basic Res. Cardiol.* **2006**, *101*, 53−60.

(8) Zeng, Y.; Kaytakoglu, S.; Harrison, D. P. Reduced Cerium Oxide as an Efficient and Durable High Temperature Desulfurization Sorbent. *Chem. Eng. Sci.* **2000**, *55*, 4893−4900.

(9) Zeng, Y.; Zhang, S.; Groves, F. R.; Harrison, D. P. High Temperature Gas Desulfurization with Elemental Sulfur Production. *Chem. Eng. Sci.* **1999**, *54*, 3007−3017.

(10) Flytzani-Stephanopoulos, M.; Sakbodin, M.; Wang, Z. Regenerative Adsorption and Removal of H_2S from Hot Fuel Gas Streams by Rare Earth Oxides. *Science* **2006**, *312*, 1508−1510.

(11) Kempegowda, R. S.; Laosiripojana, N.; Assabumrungrat, S. High Temperature Desulfurization over Nano-Scale High Surface Area Ceria for Application in SOFC. *Korean J. Chem. Eng.* **2008**, *25*, 223−230.

(12) Kay, D. A. R.; Wilson, W. G.; Jalan, V. High Temperature Thermodynamics and Applications of Rare Earth Compounds Containing Oxygen and Sulfur in Fuel Gas Desulfurization and SO_2 and NO_x Removal. *J. Alloy. Compd.* **1993**, *193*, 11−16.

(13) Kay, D. A. R.; Wilson, W. G. Cerium Oxide Solutions for the Desulfurization of Gases. United States Patent, 1994, No. US5326737.

(14) Mullins, D. R.; McDonald, T. S. Adsorption and Reaction of Hydrogen Sulfide on Thin-Film Cerium Oxide. *Surf. Sci.* **2007**, *601*, 4931−4938.

(15) Liu, B.; Xu, H. Y.; Zhang, Z. H. Temperature-Programmed Surface Reaction Study of Adsorption and Reaction of H_2S on Ceria. *Chin. J. Catal.* **2012**, *33*, 1631−1635.

(16) Koyuncu, D. D. E.; Yasyerli, S. Selectivity and Stability Enhancement of Iron Oxide Catalyst by Ceria Incorporation for Selective Oxidation of H_2S to Sulfur. *Ind. Eng. Chem. Res.* **2009**, *48*, 5223−5229.

(17) Chen, H. T.; Choi, Y. M.; Liu, M. L.; Lin, M. C. A First-Principles Analysis for Sulfur Tolerance of CeO_2 in Solid Oxide Fuel Cells. *J. Phys. Chem. C* **2007**, *111*, 11117−11122.

(18) Cheng, Z.; Sherman, B. J.; Lo, C. S. Carbon Dioxide Activation and Dissociation on Ceria (110): A Density Functional Theory Study. *J. Chem. Phys.* **2013**, *138* (014702), 1−12.

(19) Ling, L. X.; Zhang, R. G.; Han, P. D.; Wang, B. J. DFT Study on the Sulfurization Mechanism during the Desulfurization of ZnO Desulfurizer. *Fuel Process. Technol.* **2013**, *106*, 222−230.

(20) Song, J. J.; Niu, X. Q.; Ling, L. X.; Wang, B. J. A Density Functional Theory Study on the Interaction Mechanism between H_2S and α-Fe_2O_3(0001) Surface. *Fuel Process. Technol.* **2013**, *115*, 26−33.

(21) Zhang, R. G.; Liu, H. Y.; Li, J. R.; Ling, L. X.; Wang, B. J. A Mechanistic Study of H_2S Adsorption and Dissociation on Cu_2O(111) Surfaces: Thermochemistry, Reaction Barrier. *Appl. Surf. Sci.* **2012**, *258*, 9932−9943.

(22) Marrocchelli, D.; Yildiz, B. First-Principles Assessment of H_2S and H_2O Reaction Mechanisms and the Subsequent Hydrogen Absorption on the CeO_2(111) Surface. *J. Phys. Chem. C* **2012**, *116*, 2411−2424.

(23) Yang, Z. X.; Wang, Q. G.; Wei, S. Y.; Ma, D. W.; Sun, Q. The Effect of Environment on the Reaction of Water on the Ceria (111) Surface: A DFT + U Study. *J. Phys. Chem. C* **2010**, *114*, 14891−14899.

(24) Fronzi, M.; Piccinin, S.; Delly, B.; Traversa, E.; Stamp, C. Water Adsorption on the Stoichiometric and Reduced CeO_2(111) Surfaces: A First-Principles Investigation. *Phys. Chem. Chem. Phys.* **2009**, *11*, 9188−9199.

(25) Kumar, S.; Schelling, P. K. Density Functional Theory Study of Water Adsorption at Reduced and Stoichiometric Ceria (111) Surface. *J. Chem. Phys.* **2006**, *125*, 204704(1−8).

(26) Mayernick, A. D.; Janik, M. J. Methane Activation and Oxygen Vacancy Formation over CeO_2 and Zr, Pd Substituted CeO_2 Surfaces. *J. Phys. Chem. C* **2008**, *112*, 14955−14964.

(27) Nolan, M.; Parker, S. C.; Watson, G. W. The Electronic Structure of Oxygen Vacancy Defects at the Low Index Surfaces of Ceria. *Surf. Sci.* **2005**, *595*, 223−232.

(28) Zhou, K. B.; Wang, X.; Sun, X. M.; Peng, Q.; Li, Y. D. Enhanced Catalytic Activity of Ceria Nanorods from Well-Defined Reactive Crystal Planes. *J. Catal.* **2005**, *229*, 206−212.

(29) Aneggi, E.; Llorca, J.; Boaro, M.; Trovarelli, A. Surface-Structure Sensitivity of CO Oxidation over Polycrystalline Ceria Powders. *J. Catal.* **2005**, *234*, 88−95.

(30) Kresse, G.; Hafner, J. Ab Initio Molecular Dynamics for Liquid Metals. *Phys. Rev. B* **1993**, *47*, 558−561.

(31) Kresse, G.; Furthmüller, J. Efficient Iterative Schemes for Ab Initio Total-Energy Calculations Using a Plane-Wave Basis Set. *Phys. Rev. B* **1996**, *54*, 11169−11186.

(32) Blöchl, P. E. Projector Augmented-Wave Method. *Phys. Rev. B* **1994**, *50*, 17953−17979.

(33) Kresse, G.; Joubert, D. From Ultrasoft Pseudopotentials to the Projector Augmented-Wave Method. *Phys. Rev. B* **1999**, *59*, 1758−1775.

DOI: 10.1021/jp511289k
J. Phys. Chem. C 2015, 119, 7678−7688

(34) Perdew, J. P.; Burke, K.; Ernzerhof, M. Generalized Gradient Approximation Made Simple. *Phys. Rev. Lett.* **1996**, *77*, 3865−3868.
(35) Monkhorst, H. J.; Pack, J. D. Special Points for Brillouin-Zone Integrations. *Phys. Rev. B* **1976**, *13*, 5188−5192.
(36) Dudarev, S. L.; Botton, G. A.; Savrasov, S. Y.; Humphreys, C. J.; Sutton, A. P. Electron-Energy-Loss Spectra and the Structural Stability of Nickel Oxide: An LSDA+U Study. *Phys. Rev. B* **1998**, *57*, 1505−1509.
(37) Nolan, M.; Grigoleit, S.; Sayle, D. C.; Parker, S. C.; Watson, G. W. Density Functional Theory Studies of the Structure and Electronic Structure of Pure and Defective Low Index Surfaces of Ceria. *Surf. Sci.* **2005**, *576*, 217−229.
(38) Fabris, S.; de Gironcoli, S.; Baroni, S.; Vicario, G.; Balducci, G. Taming Multiple Valency with Density Functionals: A Case Study of Defective Ceria. *Phys. Rev. B* **2005**, *71*, 041102(1−4).
(39) Fabris, S.; Vicario, G.; Balducci, G.; de Gironcoli, S.; Baroni, S. Electronic and Atomistic Structures of Clean and Reduced Ceria Surfaces. *J. Phys. Chem. B* **2005**, *109*, 22860−22867.
(40) Loschen, C.; Carrasco, J.; Neyman, K. M.; Illas, F. First-Principles LDA + U and GGA + U Study of Cerium Oxides: Dependence on the Effective U Parameter. *Phys. Rev. B* **2007**, *75*, 035115(1−8).
(41) Nolan, M.; Parker, S. C.; Watson, G. W. CeO_2 Catalysed Conversion of CO, NO_2 and NO from First Principles. *Phys. Chem. Chem. Phys.* **2006**, *8*, 216−218.
(42) Scanlon, D. O.; Galea, N. M.; Morgan, B. J.; Watson, G. W. Reactivity on the (110) Surface of Ceria: A GGA+U Study of Surface Reduction and the Adsorption of CO and NO_2. *J. Phys. Chem. C* **2009**, *113*, 11095−11103.
(43) Huang, M.; Fabris, S. CO Adsorption and Oxidation on Ceria Surfaces from DFT+U Calculations. *J. Phys. Chem. C* **2008**, *112*, 8643−8648.
(44) Kummerle, E. A.; Heger, G. The Structures of C-$Ce_2O_{3+\delta}$, Ce_7O_{12}, and $Ce_{11}O_{20}$. *J. Solid State Chem.* **1999**, *147*, 485−500.
(45) Yang, Z. X.; Wang, Q. G.; Wei, S. Y. The Synergistic Effects of the Cu-CeO_2(111) Catalysts on the Adsorption and Dissociation of Water Molecules. *Phys. Chem. Chem. Phys.* **2011**, *13*, 9363−9373.
(46) Olivier, P.; Parker, S.; Mackrodt, W. Computer Simulation of the Crystal Morphology of NiO. *Model. Simul. Mater. Sci. Eng.* **1993**, *1*, 755−760.
(47) Guo, P.; Guo, X.; Zheng, C. G. Computational Insights into Interactions between Hg Species and α-Fe_2O_3(001). *Fuel* **2011**, *90*, 1840−1846.
(48) Henkelman, G.; Jonsson, H. Improved Tangent Estimate in the Nudged Elastic Band Method for Finding Minimum Energy Paths and Saddle Points. *J. Chem. Phys.* **2000**, *113*, 9978−9985.
(49) Henkelman, G.; Uberuaga, B. P.; Jonsson, H. A Climbing Image Nudged Elastic Band Method for Finding Saddle Points and Minimum Energy Paths. *J. Chem. Phys.* **2000**, *113*, 9901−9904.
(50) Bo, T.; Lan, J. H.; Wang, C. Z.; Zhao, Y. L.; He, C. H.; Zhang, Y. J.; Chai, Z. F.; Shi, W. Q. First-Principles Study of Water Reaction and H_2 Formation on UO_2(111) and (110) Single Crystal Surfaces. *J. Phys. Chem. C* **2014**, *118*, 21935−21944.
(51) Liu, L. L.; Liu, Q.; Zheng, Y. P.; Wang, Z.; Pan, C.; Xiao, W. O_2 Adsorption and Dissociation on a Hydrogenated Anatase (101) Surface. *J. Phys. Chem. C* **2014**, *118*, 3471−3482.
(52) Padama, A. A. B.; Chantaramolee, B.; Nakanishi, H.; Kasai, H. Hydrogen Atom Absorption in Hydrogen-Covered Pd(110) (1 × 2) Missing-Row Surface. *Int. J. Hydrogen Energy* **2014**, *39*, 6598−6603.
(53) Hu, X.; Tu, R.; Wei, J. H.; Pan, C. X.; Guo, J. D.; Xiao, W. Nitrogen Atom Diffusion into TiO_2 Anatase Bulk via Surfaces. *Comput. Mater. Sci.* **2014**, *82*, 107−113.
(54) McQuarrie, D. A. *Statistical Mechanics*; University Science Books: Sausalito, CA, 2000.
(55) Clay, J. P.; Greeley, J. P.; Ribeiro, F. H.; Delgass, W. N.; Schneider, W. F. DFT Comparison of Intrinsic WGS Kinetics over Pd and Pt. *J. Catal.* **2014**, *320*, 106−117.
(56) Fajín, J. L. C.; Cordeiro, M. N. D. S.; Gomes, J. R. B. DFT Study on the Reaction of O_2 Dissociation Catalyzed by Gold Surfaces Doped with Transition Metal Atoms. *Appl. Catal. A-Gen.* **2013**, *458*, 90−102.
(57) Lide, D. R. *CRC Handbook of Chemistry and Physics*, 76th ed.; CRC Press: New York, 1996.
(58) Mei, D. H.; Deskins, N. A.; Dupuis, M.; Ge, Q. F. Density Functional Theory Study of Methanol Decomposition on the CeO_2(110) surface. *J. Phys. Chem. C* **2008**, *112*, 4257−4266.
(59) Kullgren, J.; Lu, Z. S.; Yang, Z. X.; Hermansson, K. Sulfidation and Sulfur Recovery from SO_2 over Ceria. *J. Phys. Chem. C* **2014**, *118*, 17499−17504.
(60) Chen, F.; Liu, D.; Zhang, J.; Hu, P.; Gong, X. Q.; Lu, G. Z. A DFT+U Study of the Lattice Oxygen Reactivity toward Direct CO Oxidation on the CeO_2(111) and (110) Surfaces. *Phys. Chem. Chem. Phys.* **2012**, *14*, 16573−16580.
(61) Song, W. Y.; Hensen, E. J. M. Mechanistic Aspects of the Water-Gas Shift Reaction on Isolated and Clustered Au Atoms on CeO_2(110): A Density Functional Theory Study. *ACS Catal.* **2014**, *4*, 1885−1892.
(62) Maitarad, P.; Han, J.; Zhang, D. S.; Shi, L. Y.; Namuangruk, S.; Rungrotmongkol, T. Structure−Activity Relationships of NiO on CeO_2 Nanorods for the Selective Catalytic Reduction of NO with NH_3: Experimental and DFT Studies. *J. Phys. Chem. C* **2014**, *118*, 9612−9620.
(63) Yang, Z. X.; Yu, X. Y.; Lu, Z. S.; Li, S. F.; Hermansson, K. Oxygen Vacancy Pairs on CeO_2(110): A DFT+U Study. *Phys. Lett. A* **2009**, *373*, 2786−2792.
(64) Nolan, M. Hybrid Density Functional Theory Description of Oxygen Vacancies in the CeO_2(110) and (100) Surfaces. *Chem. Phys. Lett.* **2010**, *499*, 126−130.
(65) Yin, S. X.; Ma, X. Y.; Ellis, D. E. Initial Stages of H_2O Adsorption and Hydroxylation of Fe-Terminated α-Fe_2O_3(0001) Surface. *Surf. Sci.* **2007**, *601*, 2426−2437.
(66) Yang, Z. X.; Wu, R. Q.; Zhang, Q. M.; Goodman, D. W. Adsorption of Au on an O-Deficient MgO(001) Surface. *Phys. Rev. B* **2002**, *65*, 155407(1−8).
(67) Fabris, S.; Vicario, G.; Balducci, G.; Gironcoli, S. D.; Baroni, S. Electronic and Atomistic Structures of Clean and Reduced Ceria Surfaces. *J. Phys. Chem. B* **2005**, *109*, 22860−22867.
(68) Mullins, D. R.; Albrecht, P. M.; Chen, T. L.; Calaza, F. C.; Biegalski, M. D.; Christen, H. M.; Overbury, S. H. Water Dissociation on CeO_2(100) and CeO_2(111) Thin Films. *J. Phys. Chem. C* **2006**, *116*, 19419−19428.
(69) Ling, L. X.; Wu, J. B.; Song, J. J.; Han, P. D.; Wang, B. J. The Adsorption and Dissociation of H_2S on the Oxygen-Deficient ZnO(10$\bar{1}$0) Surface: A Density Functional Theory Study. *Comput. Theor. Chem.* **2012**, *1000*, 26−32.

DOI: 10.1021/jp511289k
J. Phys. Chem. C 2015, 119, 7678−7688